

UNIVERSITY OF ARIZONA

AEROSPACE AND MECHANICAL ENGINEERING

AME 401

Supersonic Experiments Final Report

Group G

By Theo Altneu, Tyler Cook, Reed Spurling, Gavin Vetro, Carly Wingness

12/12/2024

SUMMARY

This document is the collection of information gathered from a series of supersonic wind tunnel experiments conducted in the University of Arizona (UA) Indraft Supersonic Wind Tunnel (ISWT) and the Arizona Polysonic Wind Tunnel (APWT), under the guidance of Dr. James Threadgill and the supervision of his Teaching Assistant, Adrien Bouskela, as well as operators of APWT. The experiments aim to analyze how to solve for the Mach number of a tunnel under practical testing conditions. Analysis involved the use of the geometry of the nozzle, the use of a pitot rake, and schlieren imaging of a wedge and a cone. It was found that as experimental conditions became more practical to relevant experiments, the basic numerical equations to evaluate the Mach number had an increase in error. Performing these experiments aids in the development of skills of supersonic wind tunnel testing with various measurement techniques.

NOMENCLATURE

<u>Symbol</u>	<u>Name</u>	<u>Units</u>
A	Area	(m ²)
A^*	Critical Area	(m ²)
C_d	Coefficient of Drag	-
C_p	Coefficient of Pressure	-
D	Drag	(N)
h	Wedge Height	(m)
L	Length	(m)
M	Mach Number	-
P	Pressure	(mbar) (Pa)
P_∞	Freestream Pressure	(mbar) (Pa)
P_0	Stagnation Pressure	(mbar) (Pa)
P_c	Pressure on surface	(Pa)
q	Dynamic Pressure	(mbar) (Pa)
R	Radius	(in) (m)
Re	Reynolds Number	-
Re'	Unit Reynolds Number	(Re/m)

T	Temperature	(K)
T_0	Total Temperature	(K)
u	Air Velocity	(m/s)
\bar{u}	Time-Averaged Velocity	(m/s)
u_∞	Freestream Air Velocity	(m/s)
y	Rake Distance	(m)
α	Angle of Attack	(°)
β	Shock Angle	(°)
γ	Ratio of Specific Heats	-
θ	Cone/Wedge Angle	(°)
μ	Dynamic Viscosity	(Pa·s)
ρ	Air Density	(kg/m ³)

INTRODUCTION

This report describes a series of supersonic wind tunnel experiments conducted in the University of Arizona (UA) Indraft Supersonic Wind Tunnel (ISWT) and the Arizona Polysonic Wind Tunnel (APWT) under the guidance of Dr. James Threadgill and the supervision of his Teaching Assistant, Adrien Bouskela, as well as other wind tunnel operators. The experiments performed in this lab aim to inform undergraduate aerospace engineering students how to take measurements in supersonic wind tunnels.

The ISWT is a 2D suckdown supersonic wind tunnel with a 3.2 inch tall test section. 2D simply means that the tunnel geometry, which orchestrates the acceleration of the airflow, only varies in one plane. For ISWT, the tunnel height changes while the width remains constant, slightly wider than the test section height. The terms “suckdown” and “indraft” reveal how the tunnel operates; the tunnel is arranged so that the end of the diffuser behind the test section feeds into a large vacuum tank, separated by a valve, and the front of the nozzle upstream of the test section is open to the environment. When the valve is opened the pressure difference between the tank and the open air drives the flow through the tunnel.

In the first experiment, the geometry of a converging-diverging (CD) nozzle was used to find an ideal Mach number based on the area of the tunnel and compared it to the Mach number assuming isentropic flow with the static pressure along the wall of the nozzle. Experiment 2 utilized a pitot rake to further develop Mach equations from total pressure inside the tunnel. This was analyzed using the Rayleigh-Pitot formula and the pressure difference formula. This provides a more experimental approach to finding the Mach number inside the test section of the tunnel. Then experiments 3 and 4 used schlieren imaging to better visualize what was happening in the test section. A wedge and a cone was used to find the Mach turning angle that would then be used to calculate for the Mach number. This development in the experiments helps stimulate more practical testing with an object inside the test section of the nozzle. It also provides a clearer view on the uniformity of the tunnel. Finally, testing was done in APWT using the same methods as experiment 2. This tunnel used a different nozzle geometry, which shows how this affects the Mach number and the uniformity of a different tunnel type can be analyzed.

This report contains a methods section that describes the setup and conditions of all experiments performed, a results section that contains the theoretical development and the processed data, and it concludes with a discussion and comparison of the results obtained. There are also references and appendices of the data collected attached.

The experiments described in this report have been performed before by other groups of students in the current semester’s class. Therefore, the experimental methods and analyses described are not new, but are still useful for expanding skills and knowledge about supersonic wind tunnel testing.

EXPERIMENTAL METHODS

The initial and most apparent indicator of how the airspeed will change through a wind tunnel is the tunnel geometry. Subsonic flow is accelerated by decreasing the cross sectional area, but supersonic flow is accelerated by increasing the cross sectional area, so for a tunnel section designed to accelerate flow from subsonic to supersonic, the change in tunnel area switches from decreasing to increasing, yielding a CD nozzle. The minimum tunnel area between the converging and diverging sections is the throat, and marks where the flow reaches Mach 1. The tunnel area at this point is the critical area, A^* , and is used to determine the Mach number at every other point in the flow. A simple area relationship allows the local Mach number to be estimated based on the local area and critical area.

$$\frac{A}{A^*} = \left(\frac{\gamma + 1}{2}\right)^{-\frac{\gamma+1}{2(\gamma-1)}} \frac{\left(1 + \frac{\gamma - 1}{2} M^2\right)^{\frac{\gamma+1}{2(\gamma-1)}}}{M} \quad (1)$$

Since the tunnel is 2D, the width of the tunnel cancels out, so a ratio of h/h^* can be used in place of A/A^* , where h is the local height of the tunnel, which was given in reference [1]. This model provides a fairly accurate estimate on what speed the tunnel will operate at and requires no experimentation to compute, however does not consider the friction or viscous effects of real airflow, so in practice, the real Mach number at each point will be slightly different than predicted. Various methods can be employed to determine the actual Mach number the tunnel is operating at.

The first method in this series of experiments used pressure measurements taken throughout the nozzle to calculate local Mach numbers at those points. Pressure taps evenly spaced on the flat side wall fed into a DSA 5000 Series Scanivalve pressure scanner. These pressure measurements were then converted into a corresponding Mach number using isentropic relations, assuming the stagnation pressure, P_0 , was equal to the ambient air pressure. Figure B1.1 shows the tunnel geometry and pressure tap locations.

$$\frac{P_0}{P} = \left(1 + \frac{\gamma - 1}{2} M^2\right)^{\frac{\gamma}{\gamma-1}} \quad (2)$$

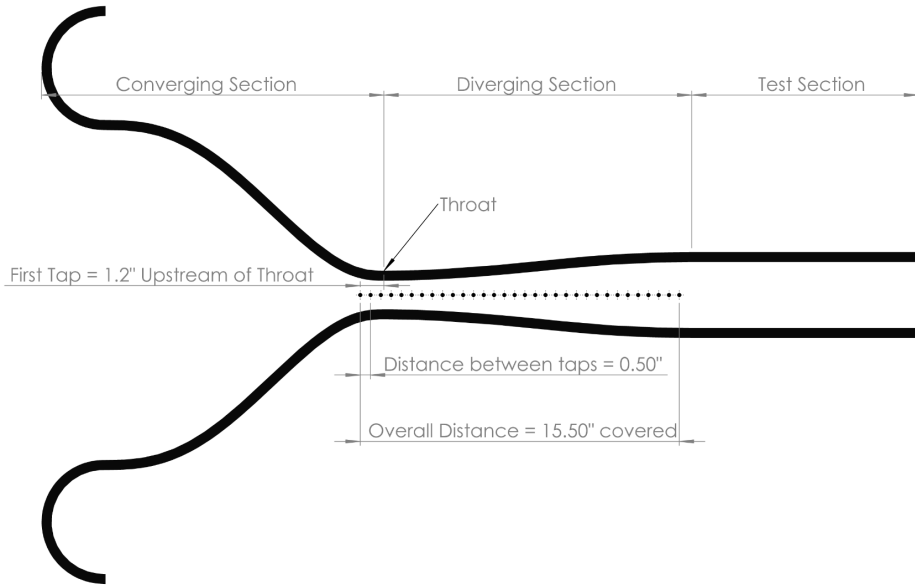


Figure B1.1. ISWT 2D geometry with pressure taps

Two runs of this experiment were completed due to the limited number of pressure taps available. The setup has 32 pressure taps, but there were only 16 lines available on the pressure scanner, thus the lines were placed on every other tap for the first run, and swapped to the unused taps for the second run, shown in Figure B1.2. The unused taps were plugged to close the leaks that would have resulted. The pressure taps at locations 10 and 11 had prior issues, and stayed plugged throughout this experiment.

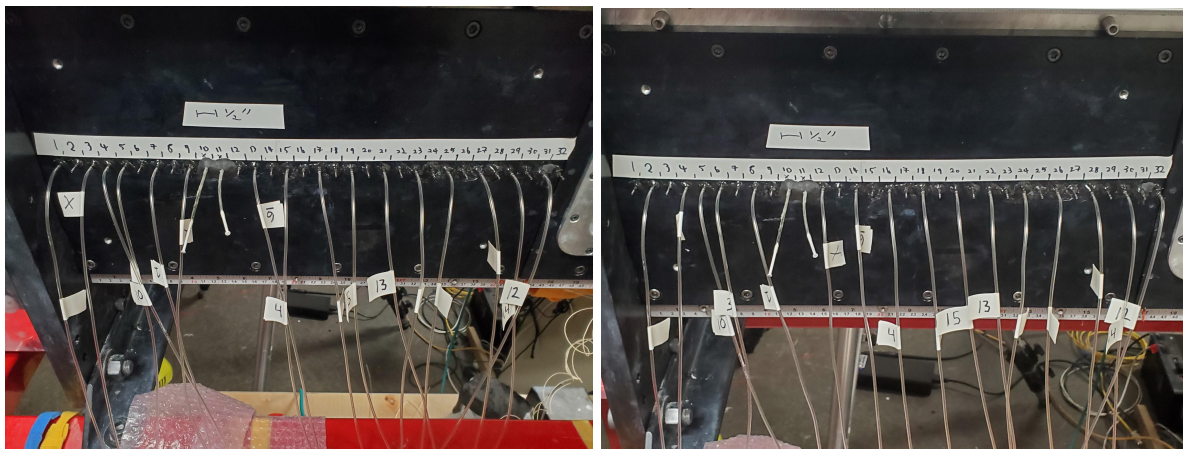


Figure B1.2. Pressure tap configuration for Run 1 (left) and Run 2 (right)

Another method of finding the real Mach flow number can be done by comparing total and static pressure. Total pressure inside the tunnel was measured using a pitot rake with seven pitot tubes spanwise. The center pitot tube is positioned in the center of the test section.

Measurements were made upstream and downstream of a test section 4 inches apart. Simultaneously, static pressure was measured through eight pressure taps along the wall of the test section around the same location of the pitot rake. The collection of data includes time-resolved total and static pressures in the test section. This data was truncated over a period of steady state pressure values for data processing. The total and static pressure measured at both locations are then used in the Rayleigh-Pitot formula:

$$\frac{P_{02}}{P_1} = \left(\frac{(\gamma-1)^2 M^2}{4\gamma M^2 - 2(\gamma-1)} \right)^{\frac{\gamma}{\gamma-1}} \frac{1-\gamma+2\gamma M^2}{\gamma+1} \quad (3)$$

where P_{02} is the total pressure experienced by the pitot probe after a shock, P_1 is the static pressure, γ is the specific heat ratio, and M is the Mach number of the airflow in the tunnel. A single static pressure location from the data set that was positioned at the same streamwise location as the rake was used in this calculation.

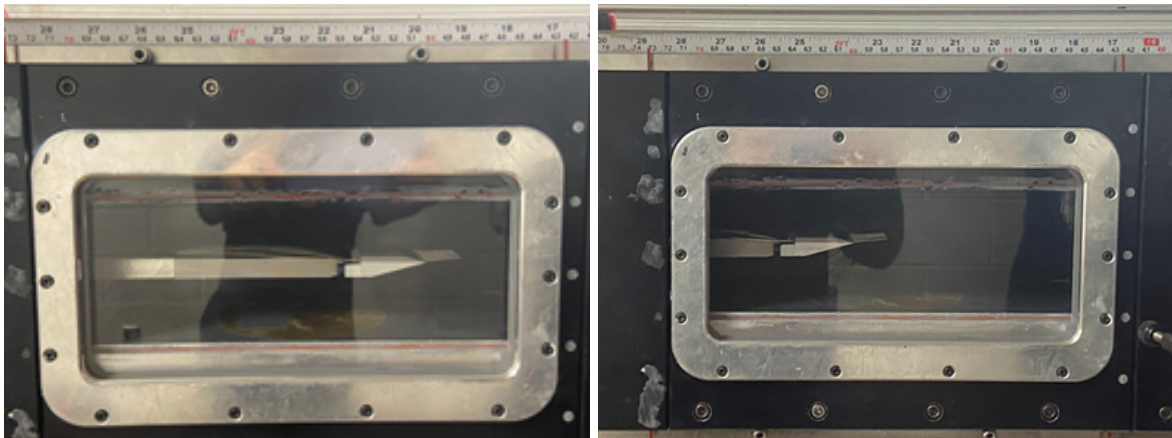


Figure B2.1: Upstream and Downstream locations of the pitot rake.

Another way to calculate the Mach number at both testing locations is to use the difference in total pressure across the pitot probe caused by the shock it experiences. This is shown by using the pressure ratio method:

$$\frac{P_{02}}{P_{01}} = \left(\frac{(\gamma+1)^2 M^2}{(\gamma-1)M^2 + 2} \right)^{\frac{\gamma}{\gamma-1}} \left(\frac{\gamma+1}{2\gamma M^2 - (\gamma-1)} \right)^{\frac{1}{\gamma-1}} \quad (4)$$

where P_{02} is the total pressure experienced by the pitot probe after a shock, P_{01} is the total pressure before the shock experienced in the tunnel, γ is the specific heat ratio, and M is the Mach number of the airflow in the tunnel. P_{01} measured was the total pressure in the room because it is an open-circuit tunnel and flow was assumed to be isentropic through the inlet and nozzle. This total pressure was 931.1 mbar for the upstream case and 930.9 mbar for the downstream case. Some total pressure was lost between runs, due to running the tunnel which slightly affected the ambient air.

The Mach number in both equations was solved for using the bisection method numerical solution. This method uses a known bounded range to find the roots of an equation as it changes sign. A tolerance of 0.001 was used, so the converged Mach number found is accurate to the inputted pressures.

Using the Equations 3 and 4 above require some assumptions to be made. The flow is assumed to be isentropic from the room through the nozzle, which allows the conservation of P_{01} . It also has to be assumed that static pressure is conserved spanwise since P_1 was measured at the wall and was used in measurements across the span of the pitot rake. It was also assumed that we have uniform flow throughout the tunnel. Finally, it was also assumed that the pitot rake is perfectly flat and experiences a normal shock. All individual errors are calculated using a 95% confidence interval.

The Mach numbers calculated with the Rayleigh-Pitot formula and the pressure difference formula allows for a comparison of methods to solve for the Mach number inside ISWT. It also will explain how uniform the flow is in the test section and if there are any discrepancies in the streamwise direction.

Experiment B3 is characterized by utilizing the ISWT coupled with optical instruments involving lights, mirrors, and cameras so as to be able to visualize the flow which will be analyzed in this portion of the lab as well as how it interacts with a presumed axisymmetric 2D wedge in the test section. The Z-Setup shown in figure B3.1 conserves space compared to other schlieren image setups, whilst still maintaining the functionality. This setup functions by shining light via mirrors in a parallel manner through the test section and allowing for those rays of light to be bent, and then ultimately focussing at a point occupied by a high-speed camera.

By taking advantage of refractive indices associated with density gradients, the knife-edge shown in this image allows for visualization of not only the second derivative of density gradients, but also the first derivative, which is what separates this method from shadowgraph imaging. This occurs as a result of some of the light being bent and consequently blocked by the aforementioned knife-edge as a result of the bending properties of light when it moves through different density mediums, which is then captured by the high speed camera sitting near the knife-edge.

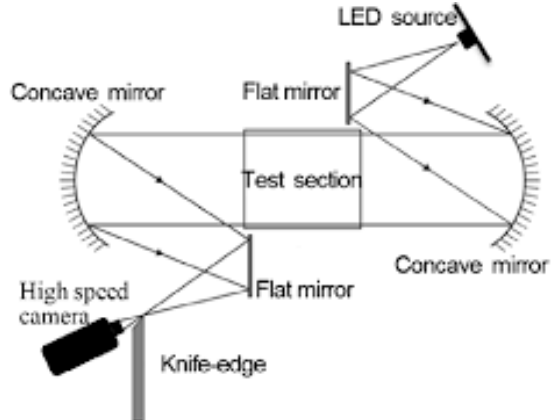


Figure B3.1: Schlieren Imaging Z-Setup

Now that the setup is complete, the data collection may begin. With the wedge placed in the test section, the tunnel may now be toggled ‘on’ and image capturing may begin. After the transient state of the flow is completed, the steady state will begin, all the while being recorded by the high-speed camera. After the steady state has been reached, the tunnel may be toggled ‘off’ and the video recording may be analyzed. One hundred frames from the steady-state were converted into one hundred individual images and saved. These one hundred images were then to be taken and uploaded into MATLAB so as to turn them into one hundred matrices with pixel brightnesses as the values. These matrices were then added together and divided by one hundred so as to create one averaged matrix that shows the steady state image averaged over the one hundred frames. This uploading and converting procedure was then applied to background images as well. Once an average background matrix has been created, this matrix was subtracted from the previously created steady state matrix so as to eliminate any optical “noise”.

Finally, one image has been created that can be analyzed to determine the shock angle associated with the flow’s interaction with a 2D wedge. By using Adobe Photoshop’s angle visualization tool, points can be drawn between the horizontal and the shock so as to determine the shock angle. By using the theta-beta-mach relationships, the angle of the wedge coupled with the determined shock angle can be used to produce the freestream mach of the tunnel.

The goal after determining the freestream mach number in the tunnel to be compared with the findings of the previous experiments was to then determine the coefficient of drag and pressure on the wedge by utilizing the definition of each of the respective coefficients as well as the wedge geometry.

The equation for the coefficient of drag across a 2D wedge is given by the following equation derived from the definition of the quantity and the wedge geometry. In equation 5, the definition of the coefficient of drag is shown.

$$C_d = \frac{D}{Lq} \quad (5)$$

The dynamic pressure can be rewritten in terms of gamma, pressure, and Mach number. Putting all of this together results in the following equation.

$$C_d = \frac{\Delta ph}{\frac{1}{2}(\gamma p_1 M_1^2)L} \quad (6)$$

Examining the difference in pressures, it can be seen that $\Delta p = p_2 - p_1$. This quantity can then be normalized by p_1 for the sake of dealing with easily found quantities with respect to supersonic flow. Additionally, the geometric quantity of h can be calculated as the following quantity: $h = 2Ltan\theta$. Putting these steps together results in the following equation:

$$C_d = \frac{\left(\frac{p_2}{p_1} - 1\right) \cdot 2Ltan\theta}{\frac{1}{2}(\gamma p_1 M_1^2) \cdot L} \quad (7)$$

By rearranging this equation and making the proper mathematical cancellations, a new form of the equation takes shape, which is exclusively dependent on quantities that are known in the system, or can be easily found. The new form of equation 7 is as follows

$$C_d = \frac{4tan\theta\left(\frac{p_2}{p_1} - 1\right)}{\gamma M_1^2} \quad (8)$$

All of the quantities in this equation are known at this point with the exception of the pressure ratio. In order to make up for this gap in knowledge, it is possible to refer to NACA 1135 for the following equation.

$$\frac{p_2}{p_1} = \frac{7M_1^2 \sin^2(\beta) - 1}{6} \quad (9)$$

This equation is solely dependent on quantities that will have already been determined from the previous portions of the lab involving Mach number, and therefore by substituting 9 into 8, the coefficient of drag can be determined.

The final step is to determine the coefficient of pressure on the face of the wedge. The following equation gives a quantity for the coefficient of pressure in terms of the wedge angle and shock angle as noted in the NACA 1135 table.

$$C_p = \frac{p_2 - p_1}{q_1} = 2 \frac{\tan(\theta)}{\tan(\theta) + \cot(\beta)} \quad (10)$$

In Experiment B4, we used the ISWT with a Mach 2.3 nozzle installed to analyze the flow behavior over a cone. After verifying that the schlieren imaging system is arranged such

that the camera can see the cone clearly in the wind tunnel test section, and is arranged correctly much like the setup shown in Figure B3.1, the wind tunnel can be turned on and allowed to run until the flow reaches a steady state for an amount of time deemed acceptable by the responsible test engineer. The high speed camera catches hundreds of frames of the flow during the wind tunnel in transient and steady states. One hundred frames from the steady state are picked out, and then processed using the MATLAB script that was also used to analyze the schlieren images in Experiment B3. This code averages the frames together and subtracts background noise for clarity. As two runs were completed, a total of two hundred and two frames were used to create the resultant image.

Now with the schlieren image, we can use Adobe Photoshop's measure tool to measure the angle of the cone and of the shock wave. These measurements were made a total of 10 so that an uncertainty level could be obtained. With the cone and shock levels, the Taylor MacColl equation must be solved for the upstream, or freestream, Mach number.

$$\frac{\gamma-1}{2} [1 - (V'_r)^2 - (\frac{dV'_r}{d\theta})^2] [2V'_r + \frac{dV'_r}{d\theta} \cot(\theta) + \frac{d^2V'_r}{d\theta^2}] - \frac{dV'_r}{d\theta} [V'_r \frac{dV'_r}{d\theta} + \frac{dV'_r}{d\theta} \frac{d^2V'_r}{d\theta^2}] = 0 \quad (11)$$

$$V' = [\frac{2}{(\gamma-1)M^2} + 1]^{-1/2} \quad (12)$$

$$V'_r = V' \cos(\theta_s - \delta) \quad (13)$$

$$V'_{\theta} = V' \sin(\theta_s - \delta) \quad (14)$$

By utilizing the Compressible Aerodynamics Calculator from Virginia Tech, the freestream Mach number can be found from the cone angle and shock angle and their uncertainty range.

There are several assumptions that must be made such that the following calculations can be valid. The assumptions are:

1. The cone is mounted perfectly horizontal to the flow, and does not bend or shift under load.
2. The Schlieren images are perfectly aligned with the test section.
3. The pressure at the base of the cone is equal to the freestream pressure.
4. Cone is semi-infinite, such that the flow depends only on the azimuthal angle.
5. Flow is axisymmetric, irrotational, and adiabatic.
6. The measured stagnation pressure of the room is assumed to be the stagnation pressure of the freestream.

With the freestream Mach number, the pressure on the surface of the cone can then be found. The equation for the surface pressure coefficient is below.

$$C_p = \frac{p_c - p_1}{q_1} = \frac{2(\frac{p_c}{p_1} - 1)}{\gamma M_1^2} \quad (15)$$

Where p_c is the pressure on the surface of the cone, p_1 is the freestream pressure, q_1 is the freestream dynamic pressure, M_1 is the freestream Mach number, and γ is the ratio of heat capacity at constant pressure to the heat capacity at constant volume. The value for $\frac{p_c}{p_1}$ is also found from the Compressible Aerodynamics Calculator. The pressure coefficient equation can be simplified into the right equation by utilizing the isentropic relationships between pressure and stagnation pressure, and dynamic pressure and stagnation pressure.

$$\frac{p}{p_0} = (1 + \frac{\gamma-1}{2}M^2)^{\frac{-\gamma}{\gamma-1}} \quad (16)$$

$$\frac{q}{p_0} = \frac{\gamma}{2}M^2(1 + \frac{\gamma-1}{2}M^2)^{\frac{\gamma}{\gamma-1}} \quad (17)$$

Finally, the coefficient of drag can be calculated. This is straightforward, as the equation for drag coefficient simplifies down to be equivalent to the surface pressure coefficient.

$$C_D = C_p = \frac{2(\frac{p_c}{p_1} - 1)}{\gamma M_1^2} \quad (18)$$

In Experiment B5, we used the APWT instead of the ISWT. The APWT is a blowdown tunnel, meaning that pressurized air from an upstream reservoir is released into the tunnel. The air first enters a settling chamber, where its total temperature and pressure are measured. The air is then accelerated by a nozzle, causing a drop in static pressure and an increase in Mach number dependent on the nozzle expansion ratio [5]. Assuming the flow through the nozzle is isentropic, there is no loss in total pressure or total temperature.

We ran the tunnel for ten seconds with a target p01 of 80 psi, measuring total pressure along a vertically oriented rake of 15 Pitot tubes. We recorded the total temperature of the flow and the total pressure ratios across normal shocks formed in front of the Pitot tubes. From this data, we calculated the distribution of Mach and Reynolds numbers in the flow across the rake. We compare these results to those we obtained from other student teams' data collected at tunnel stagnation pressures of 60 psi (from Group I) and 100 psi (from Group J).



Figure B5.1: On the left, the APWT, in AME N229. On the right, the Pitot tube rake in the wind tunnel test section, in horizontal and vertical configurations. (Images from lab manual and lecture slides)

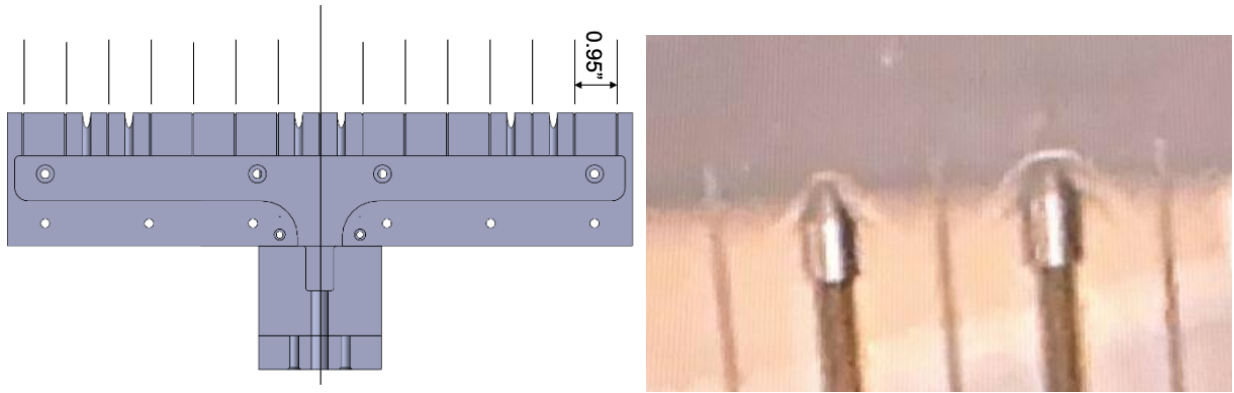


Figure B5.2: On the left, a diagram of the Pitot tube rake with 0.95" spacing between sensors. On the right, five Pitot tubes on the rake during the test, with shocks in front of each. We only collected data from the smaller-diameter tubes, though we show the larger tubes here as well due to their more clearly visible shocks.

To calculate Mach number from the pressure ratio p_{02}/p_{01} across these shocks, we solved for M in Equation (3). Once we calculated the freestream Mach number for each Pitot tube location, we used Equation (19) to find the unit Reynolds number for each.

$$Re' = \frac{\rho u}{\mu} \quad (19)$$

where ρ is air density,

$$\rho = \frac{p_1}{RT_1} \quad (20)$$

p_1 is static freestream pressure, R is the gas constant for air, 289 J/kgK, T_1 is the static freestream temperature, u is the freestream velocity,

$$u = M\sqrt{\gamma RT_1} \quad (21)$$

γ is ratio of specific heats for air, and μ is the dynamic viscosity of air,

$$\mu = \mu_0 \left(\frac{T_1}{T_{ref}} \right)^{\frac{3}{2}} \left(\frac{T_{ref} + S_\mu}{T_1 + S_\mu} \right) \quad (22)$$

Equation (22) is Sutherland's viscosity equation, where (for air), $\mu_0 = 1.716 \times 10^{-5}$ N*s/m², $T_{ref} = 273$ K, and $S_\mu = 111$ K.

RESULTS

The pressure measurements taken were plotted to reveal the pressure distribution throughout the measured section. As expected, the pressure continuously decreased as the flow accelerated through the tunnel, shown in Figure B1.3.

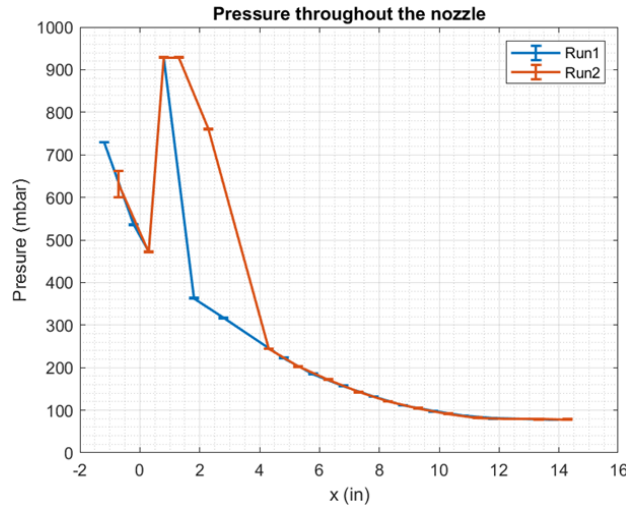


Figure B1.3. Measured pressure values in ISWT with a Mach 2.3 setup.

A smooth curve showing a gradual pressure decrease can be seen, however some significant outliers are evident. Notably, the pressure measurements from these outliers are equivalent to the ambient air pressure, indicating that there were leaks in the lines connected to those taps. The one that is slightly lower than the ambient air pressure was likely due to a very small leak which was partially influenced by the pressure in the tunnel. These points were replaced with interpolated values to continue the analysis.

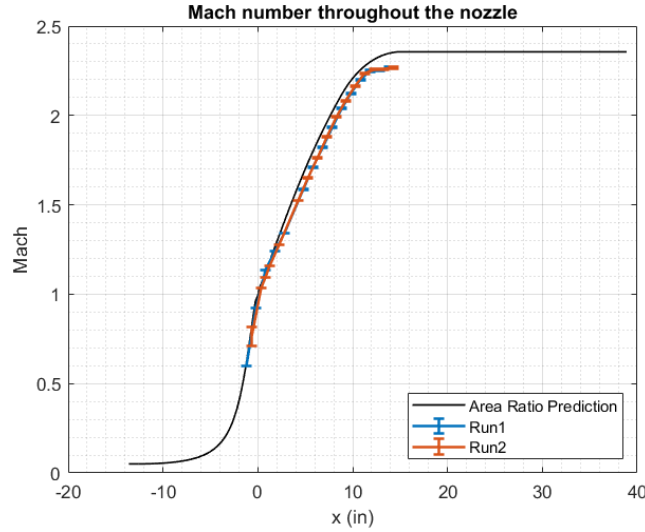


Figure B1.4. Predicted vs Calculated Mach number through the ISWT nozzle.

The Area Ratio Prediction curve in Figure B1.4 was calculated using equation (1) with the given tunnel geometry as inputs, and the Run1 and Run2 curves were generated using equation (2) with the measured pressure values as inputs. The area relationship predicted a maximum Mach number of 2.3562, but the pressure measurements only implied a maximum Mach number of 2.2684.

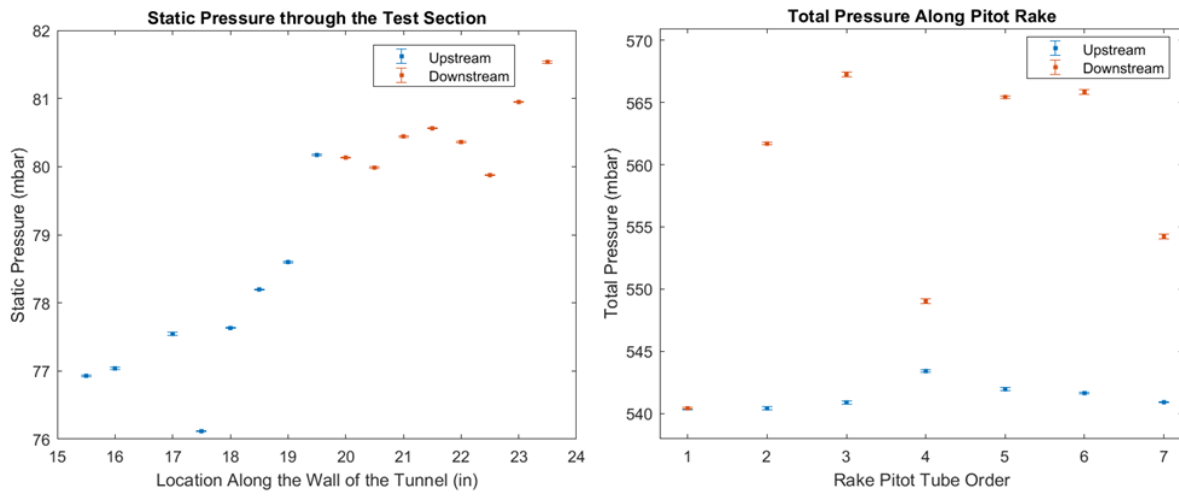


Figure B2.2 (a) and (b): Static Pressure along the wall of the tunnel and Total Pressure across a pitot rake for upstream and downstream locations.

The static and total pressure plots in Figure B2.2 show the distribution of static pressure along the wall of the tunnel and the total pressures measured by the rake in the second experiment. It can be seen that the static pressure increases along the wall of the test section. This occurs because the process is not actually isentropic and a boundary layer forms in the test section due to friction. The total pressure measured by the pitot tube also increased downstream because the strength of the shock over the tube changes from the difference in Mach number upstream and downstream. It should be noted that both of these increases are measured in mbar, so the overall change is actually very small.

It was found that the 6th static pressure port for both upstream and downstream located at 18.5 in and 22.5 in, respectively, was most in-line with the pitot rake, so that was used in the figures displayed below. A table of Mach number calculated at every static pressure port can be found in the data table appendices where the chosen static pressure is highlighted in green.

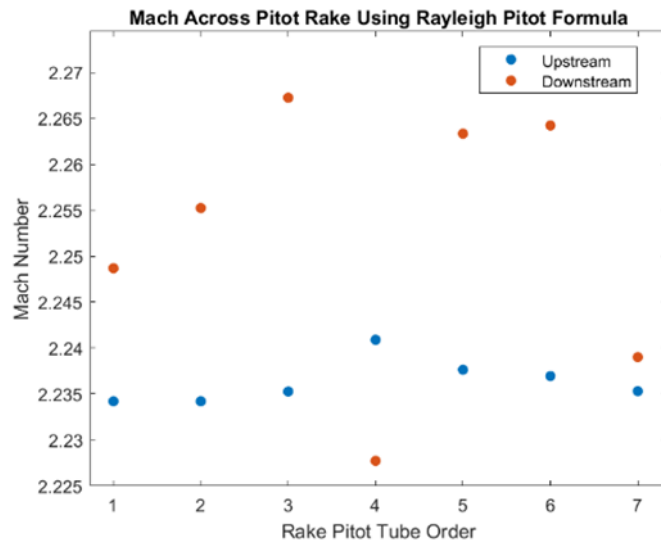


Figure B2.3: Mach number across a pitot rake using Rayleigh Pitot formula at the 6th static pressure tube both upstream and downstream.

The solution for Mach number from the Rayleigh Pitot tube has some inconsistencies across the rake. It is also seen that the downstream location experienced an overall higher Mach number than the upstream except for the center point location. Using the Rayleigh Pitot formula and neglecting the outliers of pitot 4 and 7 in the downstream case, the Mach numbers are 2.236 ± 0.00468 upstream and 2.26 ± 0.01482 downstream.

Using the pressure difference formula and neglecting the outliers of pitot 4 and 7 in the downstream case, the Mach numbers are 2.30 ± 0.00507 upstream and 2.25 ± 0.0166 downstream.

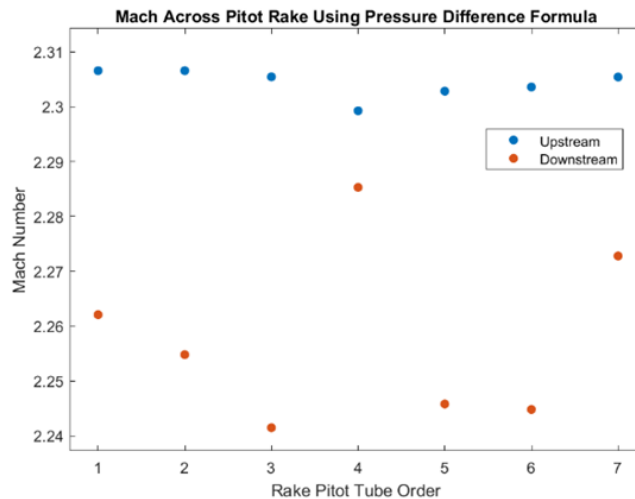
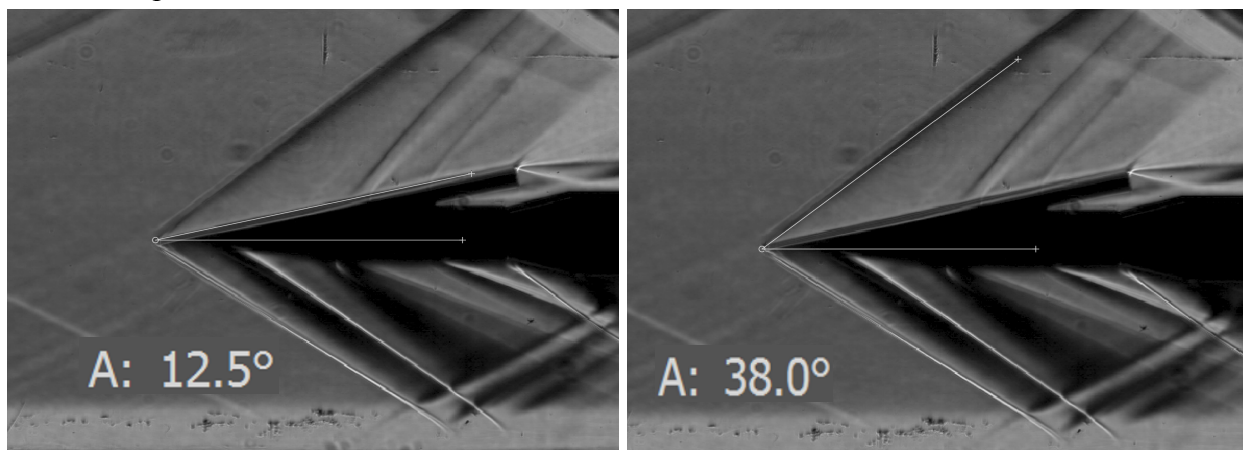


Figure B2.4: Mach number across a pitot rake using the pressure difference formula at the 6th static pressure tube both upstream and downstream.

The Mach number found using the pressure difference formula as seen in Figure B2.4 shows that the upstream case had a higher Mach number than downstream. There is still nonuniformity across the rake.

For experiment B3, the following images, B3.2 and B3.3, were produced using the aforementioned procedure to represent the averaged steady-state images with background subtraction performed.



Figures B3.2 & B3.3: Schlieren Images with Wedge and Shock Angles

From these images, the oblique shocks that are attached to the tip of the wedge can be seen, as well as a few other key aspects. Along the bottom part of the images, the boundary layer can be seen which effectively shrinks the cross-sectional area, leading to a slower than expected Mach number. Another key aspect is the shocks that can be seen in the free stream before ever meeting with the wedge. These shocks likely occur as a result of imperfections in the geometry of the inlet.

As a result of the fact that the angles are being manually measured, accuracy in measurement is a real and present source of error. In order to develop a more accurate angular reading, 10 separate attempts to read the angle were performed and then averaged to determine a tolerance reading. After these ten runs, there was a determined tolerance of approximately 0.2 degrees. The maximum and minimum wedge angles and shock angles were then used in conjunction with the developed tolerance in order to produce a range of mach numbers. The following table represents those findings.

Max/Min	Theta	Beta	Mach
Max Theta/Max Beta	12.7	38.2	2.227
Min Theta/Min Beta	12.3	37.8	2.225
Max Theta/Min Beta	12.7	37.8	2.252
Min Theta/Max Beta	12.3	38.2	2.200

Average Mach 2.226

Table B3.1: Theta-Beta-Mach Maximums and Minimums

The average mach number value was then compared to the maximum and minimum calculated mach numbers (shown in green and red respectively) in order to develop an envelope of ranges that the Mach number could fall inside with respect to measurement errors. This envelope is fully developed in table 1, which collected the Mach number findings across the different experiments.

After the freestream Mach number was determined, the next step is to determine the coefficients of both pressure and drag. The coefficient of drag was the first quantity calculated, using equation 9. By plugging in the average values for Mach number, shock angle, and wedge angle, the following is achieved.

$$\frac{p_2}{p_1} = \frac{7(2.226)^2 \sin^2(38.0) - 1}{6} \Rightarrow 2.0245$$

$$C_d = \frac{4\tan(12.5)(2.0245-1)}{1.4 \cdot (2.226)^2} \Rightarrow 0.131$$

By then using equation 10, the coefficient of pressure can be found. That equation grants the following quantity:

$$C_p = 2 \frac{\tan(12.5)}{\tan(12.5) + \cot(38.0)} \Rightarrow 0.295$$

The two hundred and two frames from the two wind tunnel runs in experiment 4 were averaged and analyzed using MATLAB. The pictures are shown below, with the average angles marked.

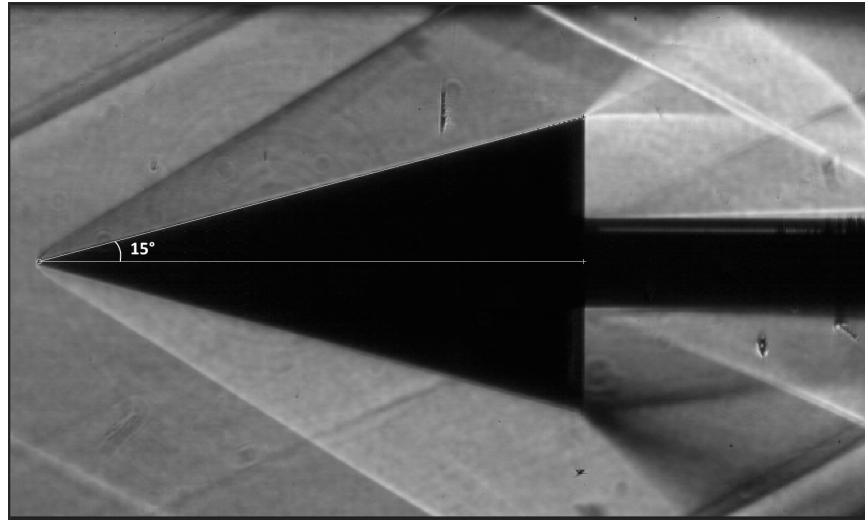


Figure B4.1: Cone Schlieren Image with Cone Angle

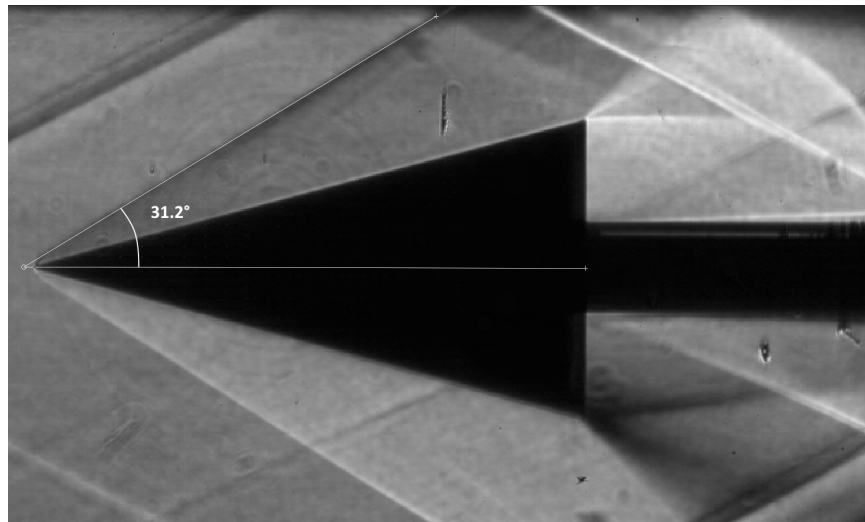


Figure B4.2: Cone Schlieren Image with Shock Angle

The cone shock angle was measured to be $15^\circ \pm 0.2^\circ$. The shock angle was measured to be $31.2^\circ \pm 0.2^\circ$. Using this range, and using the Compressible Aerodynamics Calculator, the range of freestream Mach numbers is found to be 2.216 ± 0.0305 . The range of pressure ratio of surface pressure to freestream pressure is found to be 1.67 ± 0.03 . Now, all of the information required to calculate the pressure coefficient, and therefore the drag coefficient, is found. The pressure coefficient and drag coefficient range is calculated to be 0.1953 ± 0.0141 .

The following figures represent the data collected in experiment 5 in APWT.

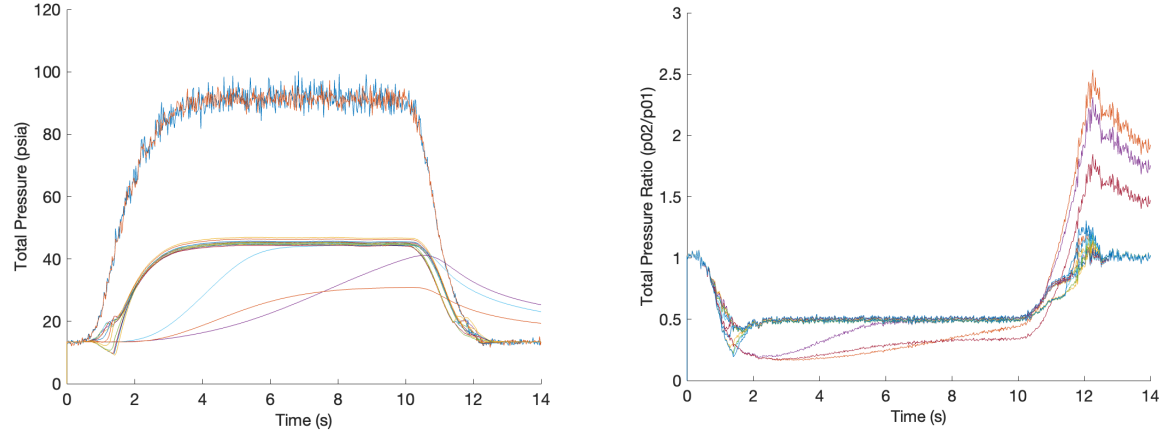


Figure B5.3: On the left are total pressures (p_0) measured during our test. The higher (~80 psi max.) p_{01} values are measured in the tunnel settling chamber, whereas the lower (~40 psi max.) total pressures (p_{02}) are measured by the Pitot tubes. On the right are the ratios between these total pressures. The three outlier curves are likely erroneous and are not included in our analysis.

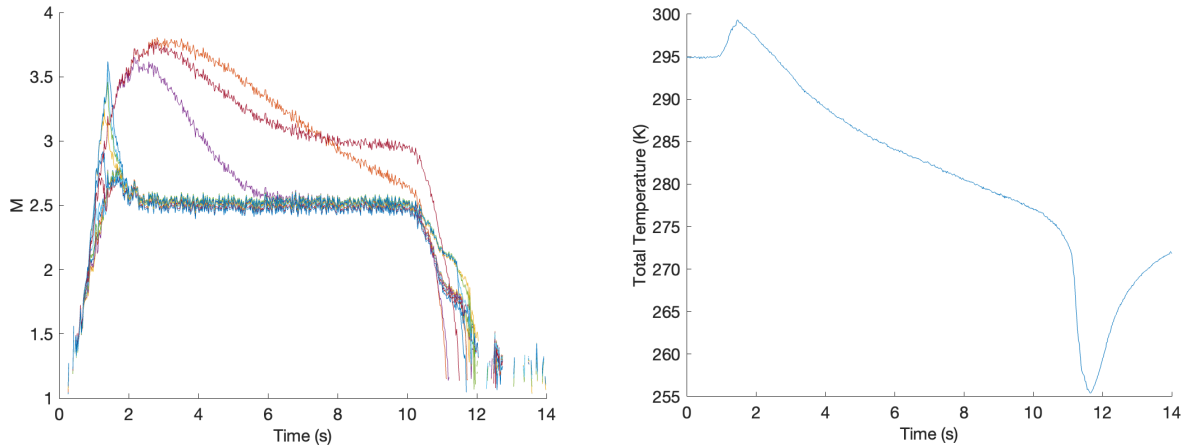


Figure B5.4: On the left, local freestream Mach numbers in the test section, calculated for each Pitot tube. On the right, unit Reynolds numbers calculated for each Pitot tube.

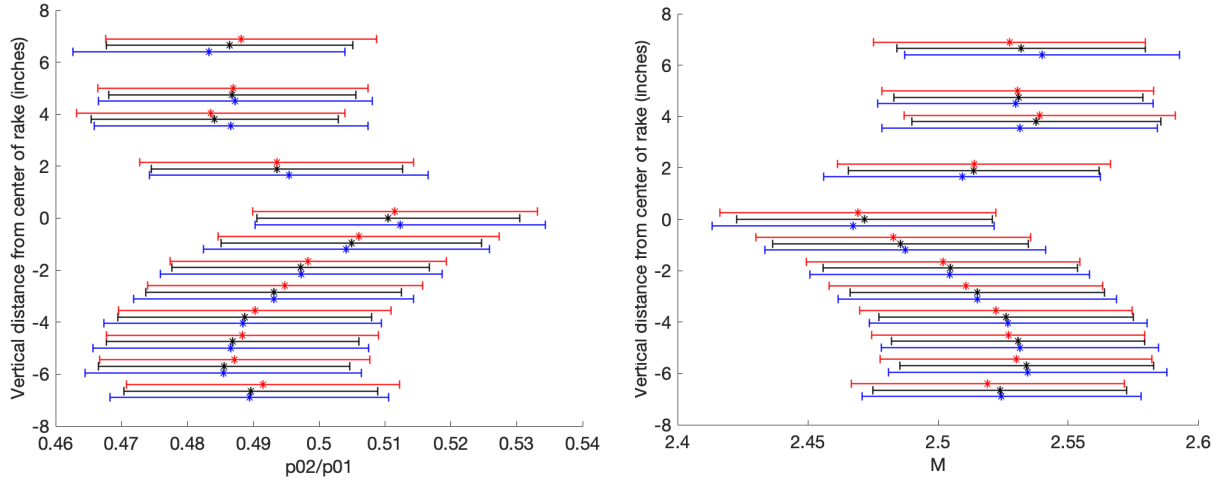


Figure B5.6: On the left, time-averaged p_{02}/p_{01} vs. Pitot tube location. On the right, time-averaged Mach number vs. Pitot tube location. With $\pm 95\%$ confidence intervals. Values from our test with a p_{01} of 80 psi, are displayed in black. Values from a 60-psi run performed later that day are shown in blue, shifted down on the plot slightly for ease of reading. Values from a 100-psi run (closer to 90 psi in practice) are shown in red. Values calculated for three likely malfunctioning Pitot tubes above the middle of the tunnel are omitted.

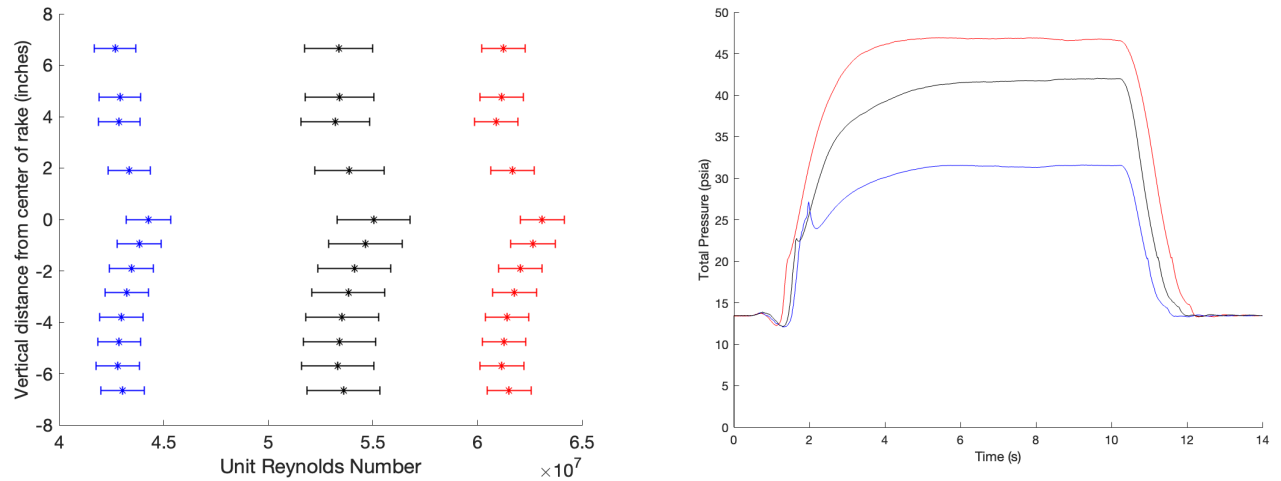


Figure B5.7. On the left, time-averaged unit Reynolds numbers (Re/m) by Pitot tube location, with 95% confidence intervals. Blue: $p_{01} = \sim 60$ psi, black: $p_{01} = \sim 80$ psi, red: $p_{01} = \sim 92$ psi. We do not observe any significant difference in the uniformity of M across these differing Reynolds numbers. On the right, total Pitot pressure (p_{02}) as measured by Pitot tube #8 (channel 16, located in the middle of the test section at $y = 0$) plotted over time for these three tests.

We note that although the tunnel was targeting a p_{01} of 100 psi in the third B5 test, it did not reach this target value. We also note that the tunnel takes a few seconds to reach its targeted operating pressure, starting at atmospheric pressure (~ 15 psia) and climbing to near steady-state after about four seconds. We therefore only considered values recorded between 4 and 9 seconds in each test when calculating averages. It takes longer for the tunnel to start and reach steady state when operating at lower total pressures/unit Reynolds numbers.

DISCUSSION

The results from the area relationship in experiment B1 imply that the tunnel was designed with viscous effects in mind, and overshot Mach 2.3 by about 0.05 Mach to account for the boundary layer build up and hopefully achieve Mach 2.3 in the center of the tunnel. While these pressure measurements indicate a lower Mach number than expected, this is likely due to fundamental flaws in this setup with the pressure taps located in the slow moving boundary layer, leading to lower calculated values for Mach number at each, with the effects of the boundary layer getting larger and larger further downstream.

Uncertainties in the measurements within the pressure scanner are not likely to contribute to this difference seen in Figure B1.4, as the reported full scale accuracy of the pressure scanner used is a minuscule 0.04% according to reference [2], which equates to 0.41 millibar. Additionally the average 95% confidence interval for each pressure tap was calculated to be ± 0.18 millibar based on the raw data from each tap, but the pressures that this tunnel is operating at are orders of magnitude larger than these error values, thus the measurements from the scanner can be assumed to be very accurate (for those without leaks).

The largest source of error in this experiment was the presence of a boundary layer at the locations being measured, which is not considered in either the area ratio relationship or the isentropic pressure relationship. While the boundary layer in supersonic flow does slow down the entire stream, its effects mostly occur near the walls of the tunnel where the measurements were being taken

This experiment concluded that Arizona's ISWT can achieve Mach numbers in the range of the designed value, however alternative methods are required to obtain values for the Mach number beyond the boundary layer.

To better understand the error in the calculated Mach numbers, an analysis of the raw pressure data in the second experiment can be done. The increase in pressure implies that there is a decrease in the area of the test section. This is due to a boundary layer forming along the wall of the tunnel from friction. The assumption that the static pressure could be conserved spanwise is not accurate because the static pressure was recorded along the wall of the tunnel inside the boundary layer. This means that the static pressure used in the Rayleigh-Pitot formula is not

actually the pressure that the pitot tube experiences. It is also noted that the pressure port located at 22.5 inches is slightly lower than its surrounding data points, which may lead to a fault in the downstream Mach number measurements in the Rayleigh-Pitot formula. The total pressure was also different upstream and downstream, which would lead to a different Mach number in the streamwise direction of the tunnel. There is some fluctuation across the span of the rake, which implies that there is some nonuniformity in the spanwise direction.

The Mach numbers shown in Figures B2.3 and B2.4 reflect this analysis. The solution for Mach number from the Rayleigh Pitot tube has some inconsistencies across the rake. It is also seen that the downstream location experienced an overall higher Mach number than the upstream except for the center point location. Understanding the expected flow physics, a boundary layer would form along the wall of the tunnel, which decreases the area and the Mach number along the test section. Therefore, using the Rayleigh Pitot formula for the data given, results in an inaccurate trend. The Mach number found using the pressure difference formula as seen in Figure B2.4 displays a more accurate trend of results. The upstream case had a higher Mach number than downstream, which is expected from the boundary layer that forms. However, there is still some discrepancy across the rake for the downstream case. The pressure difference formula only changed with total pressure experienced by the pitot tube, so it is expected that the fluctuations of the downstream case in Figures B2.3 and B2.4 likely occur from the pitot tube measurements. The pressure difference formula was the most accurate measurement method because it more correctly aligns with the expected flow physics of Mach decreasing due to a boundary layer in the test section. However, this equation uses the assumption that total pressure is conserved from the room through the tunnel, which is not the case since the tunnel is not actually isentropic. The Rayleigh Pitot method should be performed again to check its accuracy because that formula only depends on data measured directly in the tunnel.

There are some uncertainties that arise from the differences in Mach numbers that were found. The differences between the upstream and downstream Mach numbers imply that there is a boundary layer that forms along the wall of the test section. This could be due to friction against the wall and imperfections along the tunnel's surface. As the flow moves further downstream, if it is hitting any imperfections or a plug that was in the tunnel, this could cause an uneven surface that flow would "stick" to or create shocks off of. These shock interactions would also cause the nonuniformity that can be seen throughout the middle of the tunnel. This assumption was validated through the later experiments where shocks were seen in schlieren imaging upstream of the wedge and cone in experiments 3 and 4. The spanwise fluctuations are caused by the total pressure measured behind the shock experienced by the pitot tube. Shock interactions between the pitot tubes may cause these fluctuations based on their proximity to each other. Other spanwise fluctuations could be caused by a leak from fault in reattaching the pitot tube pressure lines between the upstream and downstream locations, which may explain the higher fluctuations in the downstream measurement. It was also assumed that the pitot tubes were perfectly flat and experienced a normal shock. However, by visual observation, it seems

that the rake was slightly bent upward. This would cause an oblique shock, which would mean the formulas used to calculate the Mach number would be invalid. Another uncertainty is caused by only performing one test at each test location. Performing more tests would allow a change of pressure tube locations, so that an average result could be made to rid of the impact of a faulty pressure tube.

Experiment B3 provides a visual representation of the shock waves that pass over a 2D flow. Looking at table 2 that provides a direct comparison between the different Mach number quantities calculated demonstrates the percent differences between the determined theoretical value from experiment B1 and the remainder of the experiments on the ISWT. There is an increase in differences across the experiments as they proceed. This increase in difference does not necessarily suggest that the experiments are getting worse as they go on, but rather may indicate that as the experiments consider more and more dynamics within the system, it becomes more and more difficult to get a perfectly accurate reading when compared against an expected theoretical value.

This increase in error across the various experiments, whilst slight, can point to a few things. In the first experiment, the error is as a result of imperfections in the geometry of the wind tunnel and the readings are taking into account the shear forces and boundary layer interactions as the pressure taps read the static pressure. In the second experiment the flow itself is being considered as a rake is placed into the flow, granting additional information about stagnation pressure, but considering more information about the flow. In the third experiment, the wedge itself is a larger body than the rake, and influences the flow in a different way, and the data processing considers the interactions that occur as a result of pressure drag in the wake of the shocks interacting with the wedge.

Despite the fact that each experiment seems to be compounding error, the additional complexity being added in each experiment develops a more complete and practical picture of the supersonic flow occurring in the tunnel. As a result of this, each of the sets of data is reliable for different intentions.

Error in this experiment likely comes from a combination of the boundary layer and shear force interactions found near the wind tunnel wall, as well as due to the turbulent flow that occurs in the wake of the wedge. Additionally there is an amount of error associated with the imaging itself due to the distortion of the image, or general dirtiness of the mirrors and images. To account for this, efforts were made to eliminate the background noise so that the only image left was the shock and its interaction with the assumed 2D wedge.

These results demonstrate that experiment three is a reliable indicator of the interaction of flow with a presumed 2D wedge and the pressure drag that occurs in the wake of the shock. In conclusion, the different experiments begin to slowly develop more practical applications that in

turn lead to a trade-off in the amount of possible accuracy as a result of the more complex dynamics and assumptions that need to be made.

Schlieren imaging works based on the deflection of light as they pass through regions with different refractive indices. These variations occur as a result of change in density and temperature. They provide a clear picture of compressibility effects, namely shock waves. Schlieren imaging works by using a light source focused into the test section, a mirror to collect the light and reflect it into the test section, and a second mirror to collect the light after the test section and point it into the high speed camera. Before the light reaches the high speed camera, a knife edge is used at the focal point to block part of the refracted rays. This selective blocking creates regions of varying brightness and contrast in the image, making the image clearer to read and analyze.

While all experiments provide a realistic result of freestream Mach, Experiment B4 provides the most practical value for freestream Mach, as it is representative of the 3D case. 3D geometries are used in real life applications, such as missiles or space launch vehicles. It is important to note how the more complicated 3D geometries and flow interaction affects the calculation for the freestream Mach. In experiments revolving real world applications, such as nose cone geometries for a missile, it would be more prudent to refer to the Experiment B4 result than to any others.

The source of the uncertainty in the results from Experiment B4 comes from several factors. First, the boundary layer effects from the cone affect how the shock waves are formed, and since the cone is 3D, the boundary layers are more complicated than in a 2D case. Since it was assumed that the schlieren imaging system takes a perfectly aligned picture, and that the cone does not flex or bend under load, there is the possibility that the images are not perfectly aligned, or that there are smudges or optical errors with the mirrors and lenses themselves. However, the pictures were checked for alignment by measuring the angle of the walls visible in the frames with respect to a truly horizontal line. The images were confirmed to be horizontal. Additionally there is the shear force interaction near the wind tunnel walls affecting the flow parameters near the wall, however since the cone is centered, this is unlikely to cause any error. Finally, the largest source of uncertainty is in the angle measurement itself. Measuring multiple points of the cone wall and shockwave results in several different angles. These angles are averaged together and given an uncertainty range such that all possible combinations of angles are covered.

Experiment B5, conducted in the APWT, provides an opportunity to compare results between two wind tunnels with different-size test sections. We used the same pressure-difference formula used in experiment B2 in the ISWT, and found that in B5 as in B2, there was a small but significant difference between the Mach number measured and the Mach number predicted from the isentropic Area-Mach relation. These differences may be due to 1) the formation of a

boundary layer on the tunnel surface reducing the expansion ratio and thus reducing the test section Mach number, 2) sensor bias (though we have no evidence of this), or 3) imperfectly pointed Pitot tubes with not-perfectly-normal shocks formed in front of them.

While the accuracy of the 0–750 psi Omega pressure transducers used to measure p01 in the APWT is on the order of 0.1% full scale [3], and the accuracy of the 0–100 psi Scanivalve DSA used to measure p02 across the rake is 0.05% full scale [4], these uncertainties are eclipsed by variations in p01 (and in p02/p01) possibly caused by unsteady flow. The standard dev. of p02/p01 in “steady” state ranged from 3.71% to 3.80% of p02/p01 in our test, while the standard dev. of M in steady state ranges from 0.94% to 0.99% of M in our test. These statistical uncertainties are shown in Figures B5.6 and B5.7.

Mach Comparison

The freestream Mach number must be compared between the first four experiments. While the nozzle of the ISWT was designed to be Mach 2.3, the true ideal freestream Mach number is 2.3562, as calculated using the Area-Mach relationship in Experiment B1. The percent error of each calculated freestream Mach from the ideal 2.3562 Mach number.

Experiment	Calculation Method	Freestream Mach	% Difference from Area-Mach result
B1	Pressure-Mach Relationship	2.2684 ± 0.00340	3.58% to 3.87%
B2	Rayleigh-Pitot Formula	2.236 ± 0.00468	5.16% to 5.60%
B2	Pressure Difference Formula	2.30 ± 0.00507	2.22% to 2.67%
B3	Schlieren Imaging + Oblique Shock Relations	2.226 ± 0.0260	4.63% to 7.10%
B4	Schlieren Imaging + Conical Shock Relations	2.216 ± 0.0305	4.88% to 7.81%
B5	Pressure Difference Formula	2.50 ± 0.08	2.3% to 4.7%

Table 2: Mach Comparison

CONCLUSIONS

In this set of experiments, we first calibrated the ISWT, comparing real to theoretical performance. We then calculated Mach numbers from pressure ratios in the ISWT and later in the APWT. We calculated Mach numbers in the ISWT from schlieren images of oblique shocks on a wedge and a cone. The Mach numbers were calculated in each lab section and therefore served as the link between each of the experiments and a point to be compared. Errors across all of these experiments were comparable, but gave different indications as to the practicality of the experiments and the dynamics that they assessed. These different methods of measuring Mach numbers may be appropriate given different experimental constraints.

REFERENCES

- [1] 20170210_M2.3_R48.0IN_H1.600IN_W4.8IN_L19.250IN_HYP_3DBLfix_WALL_GEOM, AME 401 D2L, Accessed 31 October, 2024.
- [2] DSA5000_2408, AME 401 D2L, Accessed 31 October, 2024.
- [3] Omega pressure transducer example info page (I am unsure if this is the exact model used):
<https://www.omega.com/en-us/pressure-measurement/pressure-transducers/px409-series/p/PX429-750GV>
- [4] Scanivalve DSA info page:
<https://scanivalve.com/products/pressure-measurement/ethernet-intelligent-pressure-scaners/dsa3217-pressure-scanner-gas-measurement/>
- [5] 202408-APWT Data Sheet

APPENDICES

B1 Data Sheets

Pressure Tap Location	Run 1 Values	Run 2 Values	Calculated Mach number
1	729.383828120000	-	0.598169327293226
2	-	631.849375000000	0.762968080866195
3	535.985273440000	-	0.922397567403416
4	471.978906250000	471.789570310000	1.03344643818689
5	928.258593750000	928.553359370000	1.03310984616566
6	-	928.637812500000	1.09467612228845
7	362.858828120000	-	1.13716940823695
8	-	760.805468750000	1.15590580639000
9	316.684667970000	-	1.24122897030824
10	-	-	1.27836517459310
11	-	-	1.34164494923723
12	-	244.647148440000	1.52328391099932
13	222.540703120000	-	1.58782292937251
14	-	202.932519530000	1.64985585438757
15	184.992343750000	-	1.71142073731123
16	-	171.660839840000	1.76074513831171
17	156.752871090000	-	1.82022941748066
18	-	142.917548830000	1.88032804902410
19	131.824531250000	-	1.93260635069826
20	-	120.389345700000	1.99107771088130
21	111.761630860000	-	2.03884527432661
22	-	104.560869140000	2.08153743255704
23	97.9021777300000	-	2.12365627184283
24	-	91.7574511700000	2.16510528538626
25	86.7526660200000	-	2.20094904108215
26	-	82.1441503900000	2.23582390835256
27	80.5951074200000	-	2.24798669843760
28	-	79.3612402300000	2.25784347886385
29	79.4313769500000	-	2.25727908536918
30	-	79.2704199200000	2.25857505780377
31	78.0641796900000	-	2.26837215889724
32	-	78.1751562500000	2.26746448187920

*The full area relationship table was omitted because it is 659 lines long, but here's a section right as the flow reaches peak.

Tunnel height	Calculated Mach number
3.1970	2.3549
3.1974	2.3550
3.1980	2.3552
3.1984	2.3554
3.1988	2.3555

3.1992	2.3556
3.1996	2.3558
3.2000	2.3559
3.2004	2.3560
3.2008	2.3562

B2 Data Sheets

		Upstream Rayleigh Pitot Mach Numbers						
		Rake Position Number						
		1	2	3	4	5	6	7
Static Pressure Position	1	2.253969	2.253969	2.255033	2.260698	2.257402	2.25675	2.255068
	2	2.252253	2.252253	2.253317	2.258982	2.255686	2.254999	2.253351
	3	2.244322	2.244322	2.245386	2.251017	2.247755	2.247068	2.245386
	4	2.266912	2.266912	2.267977	2.273676	2.27038	2.269693	2.268011
	5	2.242983	2.242983	2.244013	2.249678	2.246382	2.245729	2.244047
	6	2.234194	2.234194	2.235258	2.240889	2.237627	2.23694	2.235292
	7	2.228014	2.228014	2.229078	2.234674	2.231413	2.230761	2.229078
	8	2.20429	2.20429	2.20532	2.210882	2.207655	2.207003	2.205355

		Upstream Pressure Difference Mach Numbers						
		Rake Position Number						
		1	2	3	4	5	6	7
		2.306566	2.306566	2.305433	2.299253	2.302824	2.303579	2.305399

		Downstream Rayleigh Pitot Mach Numbers						
		Rake Position Number						
		1	2	3	4	5	6	7
Static Pressure Position	1	2.244768	2.251326	2.263308	2.223825	2.259428	2.260321	2.235121
	2	2.247	2.253557	2.265574	2.226023	2.26166	2.262552	2.237318
	3	2.240099	2.246656	2.258604	2.219191	2.254725	2.255617	2.230452
	4	2.238314	2.244871	2.256819	2.217405	2.252905	2.253798	2.228666
	5	2.241335	2.247892	2.259874	2.220427	2.25596	2.256853	2.231688
	6	2.248682	2.255239	2.267256	2.227705	2.263342	2.264235	2.239
	7	2.232546	2.239069	2.251017	2.211672	2.247103	2.247995	2.222933
	8	2.223825	2.230349	2.242228	2.203054	2.238348	2.239241	2.214247

		Downstream Pressure Difference Mach Numbers						
		Rake Position Number						
		1	2	3	4	5	6	7
		2.262072	2.254793	2.241472	2.28528	2.245798	2.244802	2.272783

		Upstream (mbar)	Downstream (mbar)					
		1	2	3	4	5	6	7
Static Pressure Position		76.92933063		80.13263005				
	2	77.03880232		79.98562937				
	3	77.54475806		80.44314332				
	4	76.11559418		80.56221623				
	5	77.63102396		80.3601727				
	6	78.19620591		79.87519227				
	7	78.59942298		80.94813092				
	8	80.17135465		81.53616897				

		Rake Position Number						
		1	2	3	4	5	6	7
Upstream (mbar)		540.412	540.413	540.8851	543.4066	541.9432	541.642	540.8963
Downstream (mbar)		540.412	561.6938	567.2539	549.0375	565.4381	565.855	554.2147

B3 Data Sheets

Frame Count	100
-------------	-----

B4 Data Sheets

Room Stagnation Pressure	929.3 mbar
Room Temperature	19.3 °C
Run 1 Frame Count	101
Run 2 Frame Count	101

B5 Data Sheets

Statistical uncertainties on these values are shown in Figs. B5.6 and B5.7.

Tunnel p_{01} (psi):	60 (from other team)	80 (our data)	~90 (from other team)
Pitot Tube #	Average p_{01}/p_{02}	Average p_{01}/p_{02}	Average p_{01}/p_{02}
1	0.4896	0.4894	0.4915
2	0.4856	0.4854	0.4872
3	0.4869	0.4866	0.4884
4	0.4887	0.4884	0.4902
5	0.4931	0.4931	0.4948
6	0.4972	0.4973	0.4983
7	0.5049	0.5041	0.5060
8	0.5105	0.5123	0.5115
9	NaN	NaN	NaN
10	0.4936	0.4954	0.4936
11	NaN	NaN	NaN
12	0.4841	0.4866	0.4836
13	0.4868	0.4873	0.4869
14	NaN	NaN	NaN
15	0.4864	0.4832	0.4882

<i>Tunnel p01 (psi):</i>	<i>60 (from other team)</i>	<i>80 (our data)</i>	<i>~90 (from other team)</i>
Pitot Tube #	Freestream Mach #	Freestream Mach #	Freestream Mach #
1	2.5237	2.5244	2.5191
2	2.5341	2.5344	2.5300
3	2.5308	2.5315	2.5270
4	2.5261	2.5269	2.5222
5	2.5150	2.5150	2.5107
6	2.5047	2.5045	2.5019
7	2.4856	2.4875	2.4828
8	2.4717	2.4674	2.4692
9	NaN	NaN	NaN
10	2.5137	2.5092	2.5138
11	NaN	NaN	NaN
12	2.5377	2.5314	2.5392
13	2.5309	2.5298	2.5306
14	NaN	NaN	NaN
15	2.5319	2.5401	2.5275
<i>Tunnel p01 (psi):</i>	<i>60 (from other team)</i>	<i>80 (our data)</i>	<i>~90 (from other team)</i>
Pitot Tube #	Unit Reynolds # *10^7	Unit Reynolds # *10^7	Unit Reynolds # *10^7
1	5.3600	4.3029	6.1510
2	5.3318	4.2810	6.1169
3	5.3407	4.2875	6.1262
4	5.3535	4.2974	6.1412
5	5.3838	4.3233	6.1773
6	5.4122	4.3463	6.2050
7	5.4652	4.3838	6.2655
8	5.5037	4.4282	6.3086
9	NaN	NaN	NaN
10	5.3874	4.3359	6.1675
11	NaN	NaN	NaN
12	5.3217	4.2876	6.0885

13	5.3404	4.2912	6.1150
14	NaN	NaN	NaN
15	5.3377	4.2689	6.1247